Fabrication of Acid Violet 34/Nickel Hydroxide Ultrathin Film and Its Electrocatalytic Performance for Glucose

Li Chen, *Xianggui Kong*, *Dongpeng Yan*, *Min Wei*,* *Xue Duan*

State Key Laboratory of Chemical Resource Engineering, Beijing University of Chemical Technology, Beijing 100029, P. R. China
*e-mail: weimin@mail.buct.edu.cn

Received: November 29, 2011
Accepted: March 7, 2012

Abstract
This article reports the fabrication of Acid Violet 34 (AV34)/nickel hydroxide nanosheets ultrathin film on the glassy carbon electrode (GCE) via the electrostatic layer-by-layer (LBL) technique, and its electrocatalytic oxidation for glucose was demonstrated. UV-vis absorption and electrochemical impedance spectra indicate the uniform deposition of the LBL film, with a continuous and smooth film surface observed by SEM and AFM. The electrochemical performance of the ultrathin film was studied by cyclic voltammetry and chronoamperometry. The (AV34/$Ni(OH)_2)_5$ ultrathin film modified electrode displays a fast direct electron transfer attributed to the Ni^{2+}/Ni^{3+} redox couple as well as remarkable electrocatalytic activity towards the oxidation of glucose. The linear response was obtained in the range 0.5–13.5 mM ($R=0.9994$) with a low detection limit (14 μM), high sensitivity (25.9 $\mu A\,mM^{-1}\,cm^{-2}$), rapid response (less than 1 s) and excellent anti-interference properties to the species including ascorbic acid (AA), uric acid (UA), acetamidophenol (AP) and structurally related sugars. Therefore, the AV34/$Ni(OH)_2$ ultrathin film can be potentially used as a feasible electrochemical sensor for the determination of glucose.

Keywords: α-$Ni(OH)_2$ nanosheets, Electrochemistry, Glucose sensor, Self-assembly, Thin films

DOI: 10.1002/elan.201100670

Supporting Information for this article is available on the WWW under http://dx.doi.org/10.1002/elan.201100670.

1 Introduction

Glucose sensing is of practical importance in clinical chemistry, biochemistry, environmental and food chemistry [1–3]. Many approaches have been developed for precisely monitoring glucose including surface plasmon resonance [4], Raman spectroscopy [5–7], fluorecence [8], electrochemiluminescene [9,10] and electrochemical technique [11–13]. Among these methods, electrochemical sensors for glucose have attracted great attention, owing to the advantages of fast response, time efficiency, easy operation and low cost. Most previous studies on this subject involve the use of glucose oxidase (GOD), which catalyzes the oxidation of glucose to gluconolactone in the presence of oxygen, producing H_2O_2 simultaneously [14,15]. However, it is known that the operation stability of the GOD sensors strongly depends on the activity of GOD, which is seriously influenced by the pH value, temperature, humidity and toxic chemicals. To solve these problems, direct electrooxidation of glucose on different electrodes modified by metals (platinum [16], gold [17,18], copper [19]) and alloys [20–23] has also been explored. Unfortunately, these electrodes generally suffer from low sensitivity and surface poisoning from the adsorbed intermediates and chloride. Therefore, the development of suitable nonenzymatic electrochemistry sensors for glucose still remains a challenge.

Nickel hydroxide ($Ni(OH)_2$), as one of the most important transition metal hydroxides, has received increasing attention in recent years on account of its application in catalysis and energy field [24–26]. $Ni(OH)_2$ has a hexagonal layered structure with two polymorphs, α- and β-$Ni(OH)_2$ [27,28]. The layered α-$Ni(OH)_2$ is a hydroxyl-deficient phase with analogous structure of hydrotalcites [29–31], which consists of stacked positively charged $Ni(OH)_{2-x}$ layers with anions and water molecules in the interlayer gallery to restore charge neutrality. Recently, the delamination of α-$Ni(OH)_2$ into nanosheets with uniform lateral shape and homogeneous thickness has been reported by Ida et al. [32]. One of the most important and attractive applications of exfoliated nanosheets is that they serve as building blocks to construct ultrathin films with superior functionalities to traditional materials [33,34]. This therefore inspires us to take the challenge of fabricating electrochemical sensors through alternate assembly of positively charged α-$Ni(OH)_2$ nanosheets and negatively charged functional dye via the electrostatic LBL technique [35], which would exhibit the following advantages: (1) the nanometer scale control of the assembly will result in a high dispersion of α-$Ni(OH)_2$ nanosheets with uniform orientation, facilitating the electron transfer; (2) the film components and thickness can be precisely controlled with simple manipulation and versatility.

Being important electrochemical functional materials, anthraquinone (AQ) and its derivatives have already been used as mediators for the electrocatalysis of oxygen reduction [36–38], potentiometric pH sensor [39] and emitting dye material [40]. However, the application of AQ and its derivatives in aqueous solutions is greatly limited owing to the unsatisfactory stability, water pollution and biological toxicity. In this work, a new type of nonenzymatic electrochemical sensor was fabricated by alternate deposition of positively charged α-$Ni(OH)_2$ nanosheets and negatively charged Acid Violet 34 (an AQ derivative) on the glassy carbon electrode (GCE) via the electrostatic LBL assembly technique. The resulting AV34/$Ni(OH)_2$ ultrathin films (UTFs) exhibit uniform and smooth surface, whose thickness can be controlled precisely at the nanometer level by a simple, inexpensive procedure. The electrochemical behavior of the UTF modified electrode was tested and a couple of well-defined reversible redox peaks were observed and were attributed to the Ni^{2+}/Ni^{3+} couple in the α-$Ni(OH)_2$ nanosheets. In addition, the modified electrode exhibits electrocatalytic performance towards the oxidation of glucose with fast response, high sensitivity, good stability, low detection limit as well as selectivity in the presence of interfering compounds. This work provides a facile approach by incorporation of electroactive species into an inorganic matrix, which can be used as a promising method for the detection of glucose.

2 Experimental

2.1 Materials and Reagents

Acid Violet 34 (AV34) and an aqueous solution (20 %) of poly(diallydimethylammonium chloride) (PDDA, MW: 100 000–200 000) were purchased from Alfa Aesar Chemical Co. Ltd. All other chemicals including $Ni(NO_3)_2$, hexamethylenetetramine (HMT), sodium dodecyl sulfate (SDS), NaOH and D-glucose were of analytical grade and used without further purification. A solution of D-glucose (0.01 M) was prepared and allowed to mutarotate in a refrigerator overnight before use. Water purified in a Milli-Q Millipore system ($>18\,M\Omega\,cm$) was used throughout.

2.2 Fabrication of the $(AV34/Ni(OH)_2)_n$ Multilayer UTFs

The suspension of colloidal α-$Ni(OH)_2$ nanoplatelets was prepared according to the method reported previously [32]. This method involves the synthesis of layered α-$Ni(OH)_2$ intercalated with dodecyl sulfate ions (dodecyl sulfate/α-$Ni(OH)_2$) and the resulting exfoliation process. The XRD pattern and FT-IR spectrum (Supporting Information, Figure S1 and Figure S2) indicate that dodecyl sulfate ions were successfully intercalated into α-$Ni(OH)_2$ gallery with high crystallinity, which is very essential for the subsequent exfoliation process. The transmission electron microscopy (TEM) image (Figure S3) reveals that the size of the dodecyl sulfate/α-$Ni(OH)_2$ particles ranges in 400–600 nm. By dispersing the as-synthesized dodecyl sulfate/α-$Ni(OH)_2$ in formamide and heating at 40 °C for 2 days, a green colloidal suspension was obtained with clear Tyndall light scattering (Figure S4). The well-dispersed colloidal suspension was transparent and stable without any precipitation when stored in an N_2 atmosphere for ten months. A typical AFM image and section pattern of the nanosheets (Figure S5) show that the thickness of the nanosheets was ~2 nm.

The $(AV34/Ni(OH)_2)_n$ UTFs were fabricated via the electrostatic LBL assembly technique. Prior to assembly, the GCE (3 mm in diameter) was polished successively with 1.0, 0.3, and 0.05 μm alumina powder, and sonicated in 1:1 nitric acid/water solution, absolute ethanol and Milli-Q water for 1 min respectively. Quartz glass (3.0 cm × 1.0 cm) substrates were cleaned by immersing in a fresh piranha solution (H_2SO_4:H_2O_2 (30 %) = 3:1, v/v) (warning: piranha solution is very corrosive and must be treated with extreme care) for 30 min, followed by rinsing in deionized water and drying with a N_2 flow. The cleaned GCE or quartz glass substrate was alternately immersed into the negatively charged AV34 solution ($1\,mg\,mL^{-1}$) and the colloidal suspension of α-$Ni(OH)_2$ nanosheets ($1\,mg\,mL^{-1}$) for 10 min each time; the substrate was rinsed with deionized water and dried with a N_2 flow after each step. Subsequently, deposition operations for AV34 and α-$Ni(OH)_2$ nanosheets were repeated n times to obtain the $(AV34/Ni(OH)_2)_n$ UTFs (Scheme 1). The $(AV34/PDDA)_5$ UTF modified electrode, which was used as a comparison sample, was obtained by alternately immersing the GCE into the negatively charged AV34 solution and positively charged PDDA solution for five circles.

2.3 Characterization and Amperometric Measurements

XRD patterns were recorded by a Rigaku XRD-6000 diffractometer, using Cu Kα radiation ($\lambda = 0.154$ nm) at 40 kV, 30 mA. The UV-vis spectra were collected in a Shimadzu U-3000 spectrophotometer. The morphology of thin films was investigated using a scanning electron microscope (SEM ZEISS) with the accelerating voltage of 20 kV. The surface roughness was studied using the atomic force microscopy (AFM) software (Digital Instruments, Version 6.12). The electrochemical measurements were performed using a CHI 660C electrochemical workstation (Shanghai Chenhua Instrument Co., China). A conventional three-electrode system was used, including a modified GCE as the working electrode, a platinum foil as the auxiliary electrode and a saturated Hg/HgO as the reference electrode. Electrochemical impedance spectroscopy (EIS) measurements were performed on the $(AV34/Ni(OH)_2)_n$ modified electrodes in 0.1 M NaOH with 5 mM $Fe(CN)_6^{3-/4-}$ solution at a potential of +0.19 V vs. Ag/AgCl. The EIS dispersions were recorded in the frequency range 0.01–100 kHz. The solutions were purged with highly purified nitrogen for 20 min prior to measure-

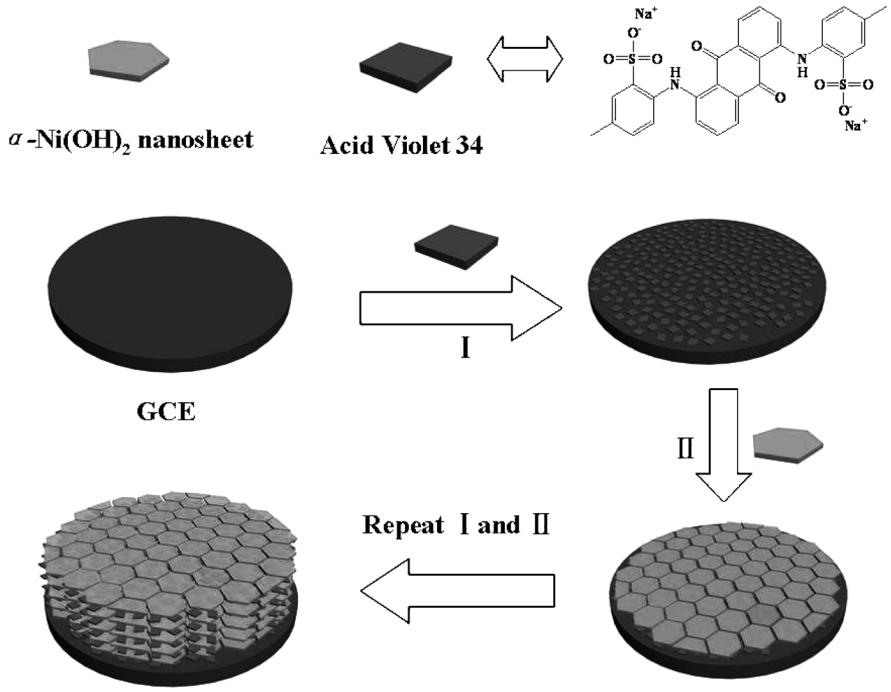

Scheme 1. Schematic representation for the LBL assembly of $(AV34/Ni(OH)_2)_n$ UTFs.

ment. All measurements were performed at room temperature.

3 Results and Discussion

3.1 Structural and Morphological Characterization of the $(AV34/Ni(OH)_2)_n$ UTFs

The fabrication process of the UTFs was monitored by UV-vis absorption spectra of quartz glass substrates coated with $(AV34/Ni(OH)_2)_n$ UTFs ($n=1$–11) as depicted in Figure 1A. The UTFs exhibit three strong absorption bands at 242, 271 and 325 nm, corresponding to the π–π* absorption bands in the anthraquinone chromophore of AV34. Another broad absorption band centered at 548 nm (in the 400–680 nm region) is due to the long axis transition of the anthraquinone ring [41]. Compared with the UV-vis absorption spectrum of the pristine AV34 in aqueous solution (Figure 1A, inset a), no obvious absorption shift was observed for the UTFs, demonstrating that AV34 molecules are accommodated between the α-$Ni(OH)_2$ nanosheets as monomer form [42]. Furthermore, the intensities of the absorption bands at 242, 271, 325 and 548 nm increased linearly with the increase of the bilayer number n (Figure 1A, inset b), indicating a stepwise and regular film growth procedure. In addition, a linear correlation between the film thickness and bilayer number was observed from their cross-sectional SEM images (Figure 1B), confirming that the UTFs possess a periodic layered structure. The thickness of one bilayer was calculated to be ~3.7 nm from the linear slope.

Surface morphology and architecture of the $(AV34/Ni(OH)_2)_n$ UTFs were further investigated by SEM and AFM. The top view SEM images (Figure 2A) for the $(AV34/Ni(OH)_2)_n$ UTFs show the film surface is continuous and uniform and the surface coverage increases with bilayer number n. The AFM topographical images (2 μm × 2 μm) show the value of root-mean square roughness (rms) increases from 1.63 nm ($n=1$) to 3.95 nm ($n=10$), indicating relatively smooth surface but decrease in uniformity along with the assembly of LBL film (Figure 2B).

3.2 Direct Electrochemistry of the UTF Modified Electrode

The electrochemical behavior of the UTF modified electrode and several comparison samples were investigated in alkaline medium. Cyclic voltammograms (CVs) of different electrodes are displayed in Figure 3. The bare electrode, pristine AV34 modified electrode and the $(AV34/PDDA)_5$ UTF modified electrode (Figure 3, curve a, b and c respectively) show no redox peaks; the pristine α-$Ni(OH)_2$ modified electrode (curve d) shows a pair of rather broad peaks with a high ΔE_p (98 mV), demonstrating a slow electron transfer which can be attributed to the Ni^{2+}/Ni^{3+} redox couple. In the case of the $(AV34/Ni(OH)_2)_5$ UTF modified electrode, a couple of well-defined oxidation peak at 0.534 V and reduction peak at 0.471 V were observed (curve e). Moreover, a rather low ΔE_p (63 mV) was obtained for the $(AV34/Ni(OH)_2)_5$ UTF modified electrode, and the ratio between the anodic and cathodic peak current was ~1.9.

Furthermore, the CVs of $(AV34/Ni(OH)_2)_n$ modified electrodes with different bilayer numbers reveal that the peak current (both anodic and cathodic) increased along

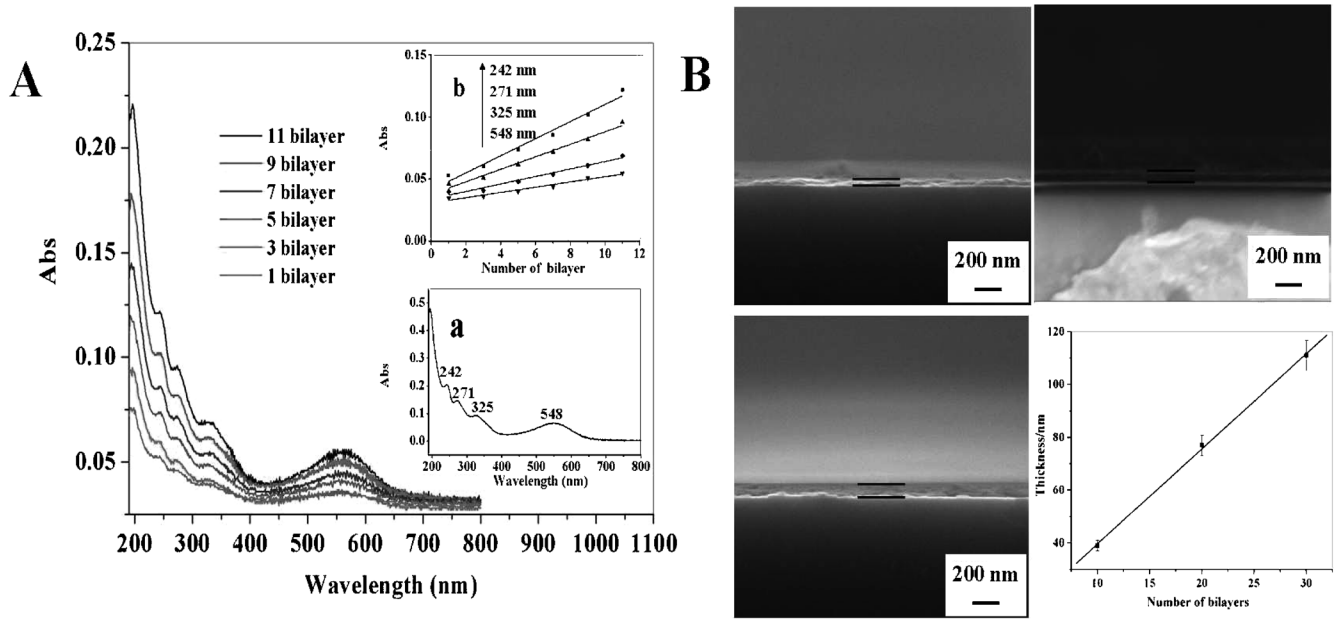

Fig. 1. (A) UV-vis absorption spectra of the $(AV34/Ni(OH)_2)_n$ UTFs along with different bilayers (n: 1, 3, 5, 7, 9, 11) on quartz glass substrates. The inset (a) shows the absorption spectrum of pristine AV34 (5×10^{-5} g mL^{-1}) and the inset (b) displays plots of the absorbance at 242, 271 325 and 548 nm vs. n respectively. (B) Side view of SEM images for the $(AV34/Ni(OH)_2)_n$ UTFs ($n=10$, 20, 30 respectively).

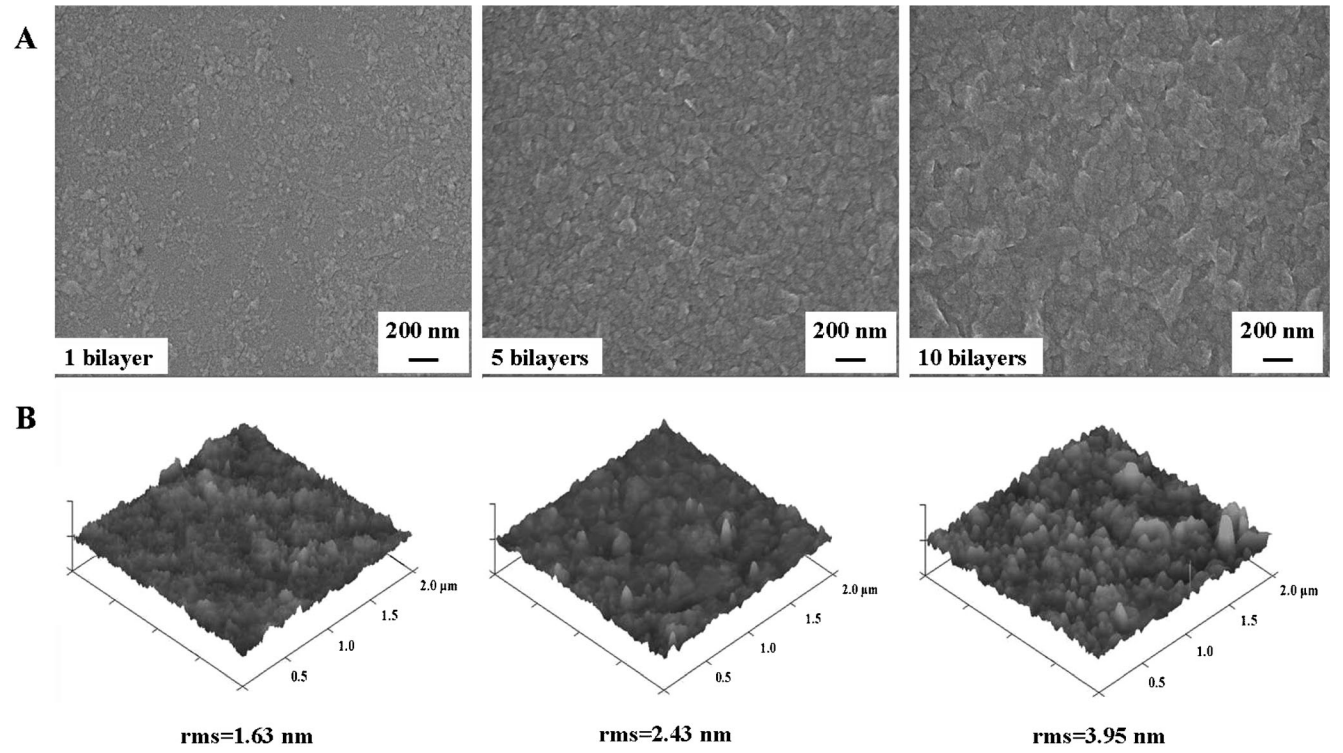

Fig. 2. (A) Top view SEM images for the $(AV34/Ni(OH)_2)_n$ UTFs ($n=1$, 5, 10). (B) AFM images for the $(AV34/Ni(OH)_2)_n$ UTFs ($n=1$, 5, 10).

with the increase of bilayer number ($n=1$–5); whilst an obvious increase in ΔE_p and small increase of the peak currents were found with further increase of bilayer number from 7 to 10 (Figure 4A). This phenomenon is attributed to the enhancement of film impedance along with the increase of film thickness [43]. Therefore, the UTF with $n=5$ was chosen as the optimum electrode for electrochemical determination of glucose in the following

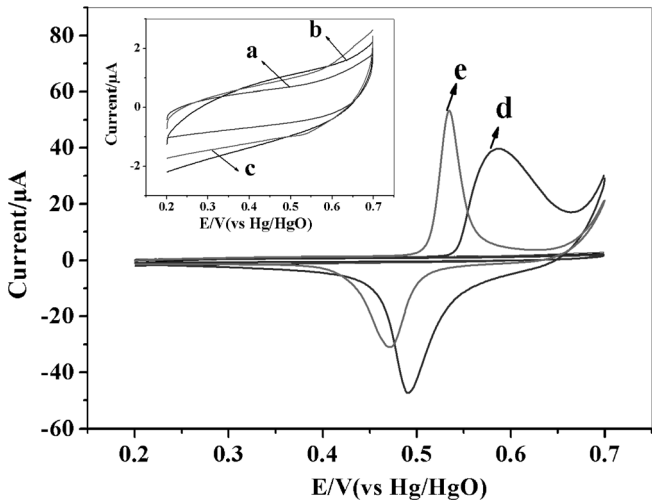

Fig. 3. CVs of (a) bare GCE, (b) pristine AV34 modified electrode, (c) the $(AV34/PDDA)_5$ modified electrode, (d) pristine α-$Ni(OH)_2$ modified electrode and (e) the $(AV34/Ni(OH)_2)_5$ modified electrode in 0.1 M NaOH at a scan rate of 0.1 $V s^{-1}$.

section. In addition, the electrochemical performance of the $(AV34/Ni(OH)_2)_5$ modified electrode was tested in NaOH solution with various concentrations (Figure S6). Negative shifts in both anodic and cathodic peak potentials were observed upon increasing the concentration of OH^-, indicating that OH^- plays a key role in the redox process of nickel.

Electrochemical impedance spectroscopy (EIS) is a powerful tool for studying the feature of a surface-modified electrode. The EIS displays two characteristic parts: the linear portion at low frequencies corresponds to the diffusion-limited process and the semicircle portion located in the higher frequencies may represent the electron-transfer limited process. In addition, the diameter of the semicircle equals the electron transfer resistance R_{et}. In this work, R_{et} reflects the restricted diffusion of the redox probe through the multilayer system, and relates directly to the accessibility of the underlying electrode or the film permeability. The Nyquist plots of the $(AV34/Ni(OH)_2)_n$ UTF modified electrodes with different bilayers are shown in Figure 4B. A semicircle part of the impedance spectrum was observed for the $(AV34/Ni(OH)_2)_n$ UTF modified electrode and the semicircle diameter increased significantly upon increasing the bilayer number. The results above further confirm a successful LBL growth of the $(AV34/Ni(OH)_2)_n$ UTF on the surface of GCE.

Figure 4C shows the effect of scan rate (0.02–0.14 V s^{-1}) on the electrochemical response of the $(AV34/Ni(OH)_2)_5$ film modified electrode. It was found that a linear relationship between the peak current and the potential sweep rate was obtained, indicating a surface-controlled process. Moreover, no obvious change in anodic and cathodic peak potentials of the $(AV34/Ni(OH)_2)_5$ UTF modified electrode was found as the scan rate increased from 0.02 to 0.14 V s^{-1}, demonstrating the AV34 accelerates the electron transfer between nickel hydroxide nanosheets and GCE. In addition, the electrochemical kinetic parameters can be calculated for a diffusionless cyclic voltammetric system. Based on Laviron theory, the electron transfer coefficient (α) and the electron transfer rate constant (k_s) for the $(AV34/Ni(OH)_2)_5$ UTF modified electrode were estimated by the following equations [44, 45]:

$$E_{pa} = E^{\theta\prime} + 2.303[RT/(1-\alpha)nF] \log \nu \quad (1)$$

$$E_{pc} = E^{\theta\prime} - 2.303\ (RT/\alpha nF) \log \nu \quad (2)$$

$$\log k_s = \alpha \log (1-\alpha) + (1-\alpha) \log \alpha - \log (RT/nF\nu) - nF\Delta E_p \alpha(1-\alpha)/2.303\ RT \quad (3)$$

where α is the charge transfer coefficient; k_s is the electron transfer rate constant; ν is the scan rate; n is number of transferred electrons; R is the gas constant; F is the Faraday constant; T is the absolute temperature; $E^{\theta\prime}$ is the apparent formal potential. From the linear relationship between E_p and log (ν/V s^{-1}) (Figure S7A), charge transfer coefficient, $\alpha = 0.65$, was obtained. Introducing the value of α in Equation 3, an apparent surface electron transfer rate constant, $k_s = 1.8\ (\pm 0.10)\ s^{-1}$ was estimated for the $(AV34/Ni(OH)_2)_5$ UTF modified electrode. Compared with the pristine α-$Ni(OH)_2$ modified electrode ($k_s = 0.7\ (\pm 0.06)\ s^{-1}$) (Figure S7B), the much larger k_s of the $(AV34/Ni(OH)_2)_5$ electrode ($1.8\ (\pm 0.10)\ s^{-1}$) indicates that AV34 enhanced the electron transfer. Furthermore, the stability of the UTFs was evaluated by consecutive voltammetric sweep method. After 20 consecutive scanning, the relative standard deviation (RSD) was 0.8 % for the anodic current and 0.4 % for the cathodic current (Figure 4D), indicating excellent stability of the $(AV34/Ni(OH)_2)_5$ UTF modified electrode.

3.3 Electrocatalytic Behavior of the $(AV34/Ni(OH)_2)_5$ UTF Modified Electrode for Glucose

In this section, the $(AV34/Ni(OH)_2)_5$ modified electrode was chosen as the optimum electrode for amperometric determination of glucose by cyclic voltammetry and chronoamperometric measurement.

In order to study the electrocatalytic reaction process, several comparison samples (the bare electrode, pristine AV34 modified electrode and the $(AV34/PDDA)_5$ UTF modified electrode) were investigated firstly. The CVs for the three comparison samples display no obvious current response in the presence of 2 mM glucose in a 0.1 M NaOH solution (Figure 5A, inset). However, in the case of the $(AV34/Ni(OH)_2)_5$ UTF modified electrode, a remarkable enhancement in oxidation current and decline in reduction current were observed upon addition of 2 mM glucose (Figure 5A); moreover, the anodic peak increases and the cathodic peak decreases gradually along with the increase of the glucose concentration (Fig-

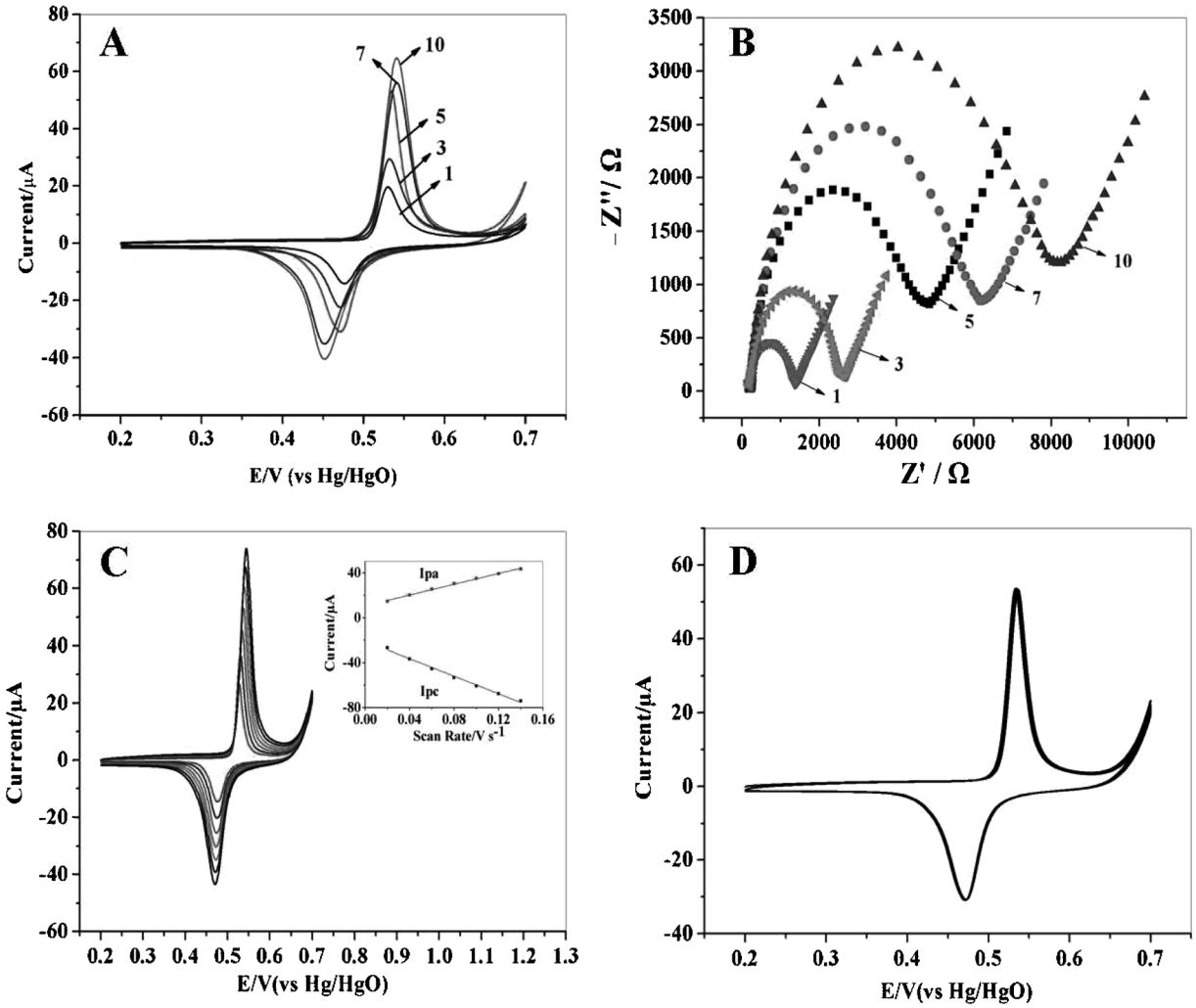

Fig. 4. (A) CVs of the $(AV34/Ni(OH)_2)_n$ modified electrode with different bilayer numbers (n): 1, 3, 5, 7 and 10 in 0.1 M NaOH at a scan rate of 0.1 $V s^{-1}$. (B) Nyquist plots of electrochemical impedance spectroscopy for the $(AV34/Ni(OH)_2)_n$ UTF modified GCE with different bilayer numbers (n): 1, 3, 5, 7 and 10 in 5 mM $Fe(CN)_6^{3-/4-}$ solution. (C) CVs of the $(AV34/Ni(OH)_2)_5$ modified electrode with scan rate ranging from 0.02 to 0.14 $V s^{-1}$. Inset: plots of peak current vs. scan rate in 0.1 M NaOH. (D) The stability of the $(AV34/Ni(OH)_2)_5$ modified electrode in 0.1 M NaOH at a scan rate of 0.1 $V s^{-1}$ for 20 consecutive cycles.

ure 5B), indicating that glucose participates and accelerates the redox reaction of $Ni(OH)_2$ on the surface of GCE. Meanwhile, positive shifts in both the oxidation and reduction potentials were also found, which can be attributed to the consumption of OH^- in the electrocatalytic reaction process as well as the diffusion limitation of glucose at the electrode surface [46]. On the basis of the results in this work and previous reports [47], it is proposed that the electrochemical reaction can be described by the following equations:

$$Ni(OH)_2 + OH^- \rightarrow NiO(OH) + H_2O + e^- \quad (4)$$

$$NiO(OH) + \text{glucose} \rightarrow Ni(OH)_2 + \text{glucolactone} \quad (5)$$

Chronoamperometric measurement was used to determine the response time, response range and stability of the $(AV34/Ni(OH)_2)_5$ modified electrode towards electrocatalysis of glucose by successively increasing the concentration of glucose at the constant potential of 0.6 V. A good linear relationship between anodic current and the concentration of glucose was observed as the concentration of glucose ranges from 0.5 to 13.5 mM, with the linear regression equation: $i_{pa}(\mu A) = 1.421 + 1.829c$ (10^{-3} M), $R = 0.9994$ (Figure 6B). The detection limit is estimated to be 14 μM (signal over noise S/N = 3). Taking into account the time cost to reach 95 % of the signal, the response time was within one second (Figure 6A, inset), indicating a fast diffusion of glucose through the UTFs. A comparison study on the amperometric response of the pristine α-$Ni(OH)_2$ modified electrode showed a much narrower linear response (0.5–3.5 mM) (Figure S8, inset) and less stable electrocatalytic activity for the oxidation of glucose (Figure S8), indicating that AV34 serves as conductive mediator which enhances the stability and conductivity of the $(AV34/Ni(OH)_2)_5$ UTF.

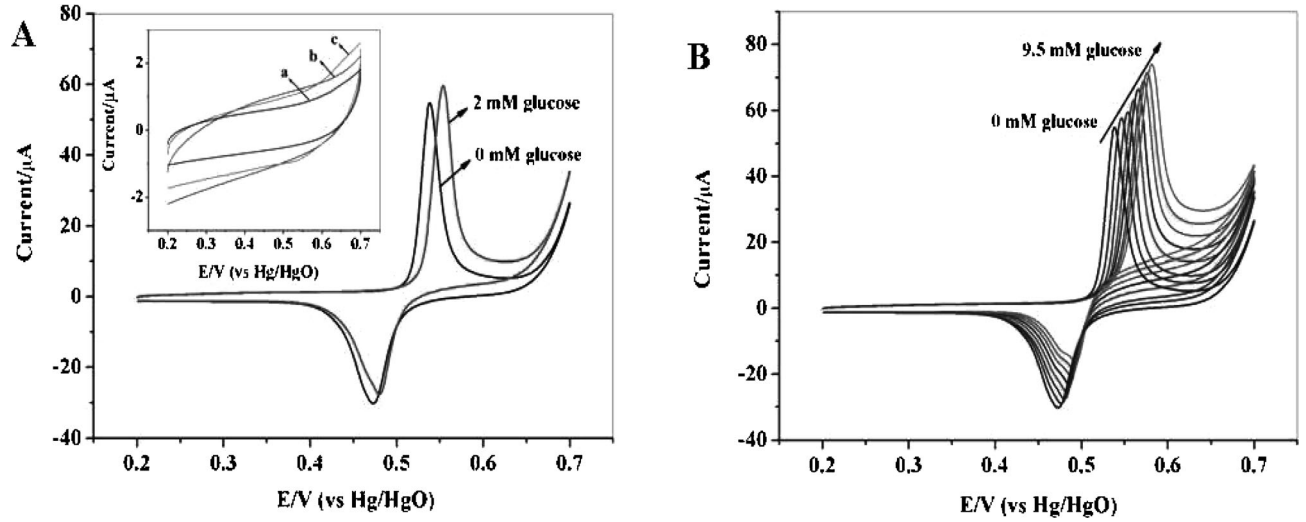

Fig. 5. (A) CVs for the $(AV34/Ni(OH)_2)_5$ UTF modified GCE in the absence and presence of 2 mM glucose, respectively. Inset: CVs for bare GCE (a), pristine AV34 modified electrode (b) and the $(AV34/PDDA)_5$ modified electrode (c) in the presence of 2 mM glucose. Scan rate: 0.1 Vs^{-1}. (B) CVs of the $(AV34/Ni(OH)_2)_5$ UTF modified GCE electrode in 0.1 M NaOH solution with different concentrations of glucose (from bottom to up: 0, 1, 2, 3.5, 5, 6.5, 8 and 9.5 mM). Scan rate: 0.1 Vs^{-1}.

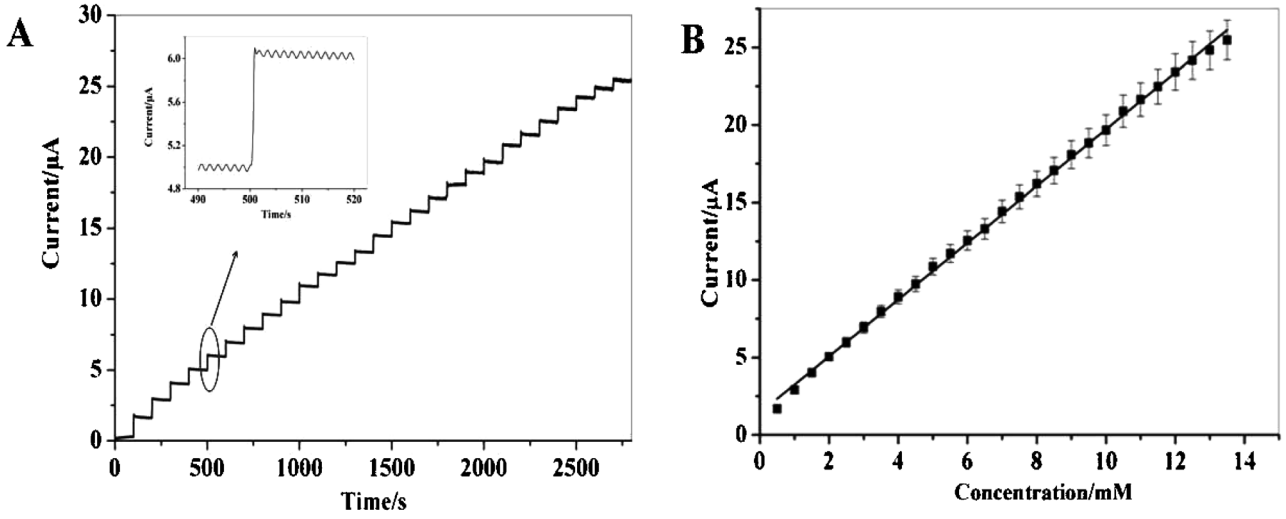

Fig. 6. (A) Typical amperometric response of the $(AV34/Ni(OH)_2)_5$ modified electrode to successive additions of 0.5 mM glucose into 0.1 M NaOH solution. Applied potential was 0.6 V. (B) The calibration curve of *I–c* obtained by chronoamperometry.

Selectivity plays a vital role for sensors in practical application owing to the presence of various interfering substrates. In the present work therefore, the interference effect of ascorbic acid (AA), uric acid (UA), acetamidophenol (AP) and structurally related sugars (maltose, fructose, galactose and xylose) was evaluated respectively during amperometric response for glucose at the $(AV34/Ni(OH)_2)_5$ UTF modified electrode. Figure 7 shows that the addition of these interference compounds does not influence the current response of glucose significantly, demonstrating that the modified electrode can selectively catalyze the oxidation of glucose. In addition, the $(AV34/Ni(OH)_2)_5$ UTF modified electrode exhibits high thermal stability (95% of its initial electrocatalytic current remained after heating at 60 °C for 1 h) and long-term stability (93% of its initial current remained after two weeks). Furthermore, the reproducibility was evaluated by fabricating five sensors independently. An acceptable reproducibility was obtained with RSD of 1.9% for direct electrochemical performance.

To evaluate the practical application of the $(AV34/Ni(OH)_2)_5$ UTF modified electrode, five sensors were further applied for the determination of glucose in blood serum samples, respectively. The serum was freshly diluted by adding 0.5 mL of serum sample to 10.0 mL of 0.1 M NaOH solution, and the current response was obtained at 0.6 V. Table 1 lists the data of glucose determination by the $(AV34/Ni(OH)_2)_5$ modified electrode, from which sat-

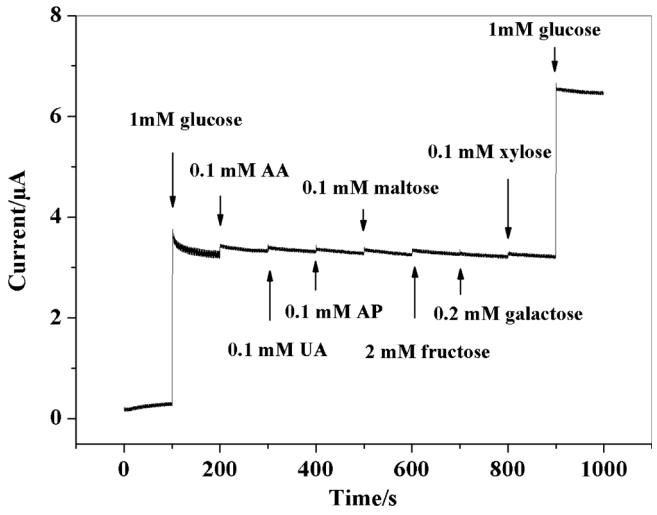

Fig. 7. Current response obtained at the $(AV34/Ni(OH)_2)_5$ UTF modified electrode for the addition of glucose and interference compounds into 0.1 M NaOH solution. Applied potential was 0.6 V.

Table 1. Determination of glucose in blood serum samples

Serum sample	Referenced values [a]	Determined values [b]	RSD (%)
1	4.28	4.43 ± 0.11	3.7
2	4.83	4.94 ± 0.05	3.9
3	6.69	6.81 ± 0.06	3.6
4	5.32	5.44 ± 0.09	3.3
5	5.87	6.09 ± 0.07	4.1

[a] Concentration (mM) obtained with hexokinase method. [b] An average concentration (mM) obtained with the modified electrode (5 independent measurements per sample with one electrode).

isfactory results were obtained compared with the hexokinase method (spectrophotometry). The above results demonstrate that the $(AV34/Ni(OH)_2)_5$ UTF modified electrode can be potentially applied in the determination of glucose.

4 Conclusions

In conclusion, multilayer films containing negatively charged AV34 and positively charged hexagonal nickel hydroxide nanosheets were successfully fabricated by electrostatic LBL technique. The structural and surface morphology studies show that the surface of UTFs are continuous and uniform. The as-prepared $(AV34/Ni(OH)_2)_5$ UTF modified electrode shows direct electrochemical performance with a couple of well-defined redox peaks attributed to Ni^{2+}/Ni^{3+} in α-$Ni(OH)_2$ nanosheets. Furthermore, the $(AV34/Ni(OH)_2)_5$ UTF modified electrode displays remarkable electrocatalytic activity towards the oxidation of glucose with a linear response range of 0.5–13.5 mM ($R = 0.9994$), a low detection limit (14 μM), high sensitivity (25.9 $\mu A\,mM^{-1}\,cm^{-2}$), rapid response (less than 1 s), good stability as well as excellent anti-interference properties to other species including AA, UA, AP and structurally related sugar. Therefore, the results demonstrate that α-$Ni(OH)_2$ nanosheet can serve as one promising building block for fabricating hybrid UTFs used as electrochemical sensor for the determination of glucose.

Acknowledgements

This work was supported by the *National Natural Science Foundation of China*, the 863 Program (Grant No. 2009AA064201), the 111 Project (Grant No. B07004) and the Collaboration Project from the Beijing Education Committee.

References

[1] S.-R. Lee, Y.-T. Lee, K. Sawada, H. Takao, M. Ishida, *Biosens. Bioelectron.* **2008**, *24*, 410.
[2] J. D. Newman, A. P. F. Turner, *Biosens. Bioelectron.* **2005**, *20*, 2435.
[3] L. Wu, X. Zhang, H. Ju, *Biosens. Bioelectron.* **2007**, *19*, 141.
[4] X. W. Shen, C. Z. Huang, Y. F. Li, *Talanta* **2007**, *72*, 1432.
[5] D. A. Stuart, J. M. Yuen, N. Shah, O. Lyandres, C. R. Yonzon, M. R. Glucksberg, J. T. Walsh, R. P. Van Duyne, *Anal. Chem.* **2006**, *78*, 7211.
[6] J. M. Yuen, N. C. Shah, J. T. Walsh Jr, M. R. Glucksberg, R. P. Van Duyne, *Anal. Chem.* **2010**, *82*, 8382.
[7] K. E. Shafer-Peltier, C. L. Haynes, M. R. Glucksberg, R. P. Van Duyne, *J. Am. Chem. Soc.* **2003**, *125*, 588.
[8] P. W. Barone, R. S. Parker, M. S. Strano, *Anal. Chem.* **2005**, *77*, 7556.
[9] P. Bertoncello, R. J. Forster, *Biosens. Bioelectron.* **2009**, *24*, 3191.
[10] X. P. Chen, H. Z. Ye, W. Z. Wang, B. Qiu, Z. Y. Lin, G. N. Chen, *Electroanalysis* **2010**, *22*, 2347.
[11] J. F. Zang, C. M. Li, X. Q. Cui, J. X. Wang, X. W. Sun, H. Dong, C. Q. Sun, *Electroanalysis* **2007**, *19*, 1008.
[12] K. E. Toghill, L. Xiao, M. A. Phillips, R. G. Compton, *Sens. Actuators B* **2010**, *147*, 642.
[13] K. E. Toghill, R. G. Compton, *Int. J. Electrochem. Sci.* **2010**, *5*, 1246.
[14] P. Du, B. Zhou, C. X. Cai, *J. Electroanal. Chem.* **2008**, *614*, 149.
[15] Y. L. Zhai, S. Y. Zhai, G. F. Chen, K. Zhang, Q. L. Yue, L. Wang, J. F. Liu, J. B. Jia, *J. Electroanal. Chem.* **2011**, *656*, 198.
[16] B. Beden, F. Largeaud, K. B. Kokoh, C. Lamy, *Electrochim. Acta* **1996**, *41*, 701.
[17] M. W. Hsiao, R. R. Adic, E. B. Yeager, *J. Electrochem. Soc.* **1996**, *143*, 759.
[18] B. K. Jena, C. R. Raj, *Chem. Eur. J.* **2006**, *12*, 2702.
[19] F. Sun, L. Li, P. Liu, Y. F. Lian, *Electroanalysis* **2011**, *23*, 395.
[20] P. Holt-Hindle, S. Nigro, M. Asmussen, A. Chen, *Electrochem. Commun.* **2008**, *10*, 1438.
[21] H. F. Cui, J. S. Ye, W. D. Zhang, C. M. Li, J. H. T. Luong, F. S. Sheu, *Anal. Chim. Acta* **2007**, *594*, 175.
[22] H. J. Qiu, X. R. Huang, *J. Electroanal. Chem.* **2010**, *643*, 39.

[23] C. Y. Tai, J. L. Chang, J. F. Lee, T. S. Chan, J. M. Zen, *Electrochim. Acta* **2011**, *56*, 3115.
[24] F. Bardé, M. R. Palacin, Y. Chabre, O. Isnard, J.-M. Tarascon, *Chem. Mater.* **2004**, *16*, 3936.
[25] F. Bardé, M. R. Palacín, B. Beaudoin, P. A. Christian, J.-M. Tarascon, *J. Power Sources* **2006**, *160*, 733.
[26] S. Ovshinsky, M. A. Feteenko, J. Ross, *Science* **1993**, *260*, 176.
[27] L. P. Xu, Y.-S. Ding, C.-H. Chen, L. L. Zhao, C. Rimkus, R. Joesten, S. L. Suib, *Chem. Mater.* **2008**, *20*, 308.
[28] B. Mavis, M. Akine, *Chem. Mater.* **2006**, *18*, 5317.
[29] A. M. Fogg, V. M. Green, H. G. Harvey, D. O'Hare, *Adv. Mater.* **1999**, *11*, 1466.
[30] A. Illaik, C. Taviot-Guého, J. Lavis, S. Commereuc, V. Verney, F. Leroux, *Chem. Mater.* **2008**, *20*, 4854.
[31] E. Scavetta, L. Guadagnini, A. Mignani, D. Tonelli, *Electroanalysis* **2008**, *20*, 2199.
[32] I. Shintaro, S. Daisuke, K. Michio, M. Yasumichi, *J. Am. Chem. Soc.* **2008**, *130*, 14038.
[33] L. Li, R. Z. Ma, Y. Ebina, K. Fukuda, K. Takada, T. Sasaki, *J. Am. Chem. Soc.* **2007**, *129*, 8000.
[34] D. P. Yan, J. Lu, M. Wei, J. B. Han, J. Ma, F. Li, D. G. Evans, X. Duan, *Angew. Chem. Int. Ed.* **2009**, *121*, 3119.
[35] W. Zhao, J. J. Xu, H. Y. Chen, *Electroanalysis* **2006**, *18*, 1737.
[36] M. Kullapere, J. M. Seinberg, U. Mäeorg, G. Maia, D. J. Schiffrin, K. Tammeveski, *Electrochim. Acta* **2009**, *54*, 1961.
[37] J. M. Seinberg, M. Kullapere, U. Mäeorg, F. C. Maschion, G. Maia, D. J. Schiffrin, K. Tammeveski, *J. Electroanal. Chem.* **2008**, *624*, 151.
[38] A. Sarapuu, K. Vaik, D. J. Schiffrin, K. Tammeveski, *J. Electroanal. Chem.* **2003**, *541*, 23.
[39] K. K. Shiu, F. Y. Song, H. P. Bait, *Electroanalysis* **1996**, *8*, 1160.
[40] S. Das, A. J. Pal, *Appl. Phys. Lett.* **2000**, *76*, 1770.
[41] K. Ray, H. Nakahara, *Phys. Chem. Chem. Phys.* **2001**, *3*, 4784.
[42] W. Y. Shi, M. Wei, J. Lu, F. Li, J. He, D. G. Evans, X. Duan, *J. Phys. Chem. C* **2008**, *112*, 19886.
[43] J. B. Han, X. Y. Xu, X. Y. Rao, M. Wei, D. G. Evans, X. Duan, *J. Mater. Chem.* **2011**, *21*, 2126.
[44] A. Salimi, H. Mamkhezri, R. Hallaj, S. Zandi, *Electrochim. Acta* **2007**, *52*, 6097.
[45] E. Laviron, *J. Electroanal. Chem.* **1974**, *52*, 355.
[46] Y. Mu, D. L. Jia, Y. Y. He, Y. Q. Miao, H. L. Wu, *Biosens. Bioelectron.* **2011**, *26*, 2948.
[47] A. Safavi, N. Maleki, E. Farjami, *Biosens. Bioelectron.* **2009**, *24*, 1655.

